



This is a repository copy of *A smart radar absorber based on the phase-switched screen* .

White Rose Research Online URL for this paper:  
<http://eprints.whiterose.ac.uk/801/>

---

**Article:**

Chambers, B. and Tennant, A. (2005) A smart radar absorber based on the phase-switched screen. *IEEE Transactions on Antennas and Propagation*, 53 (1 (par)). pp. 394-403. ISSN 0018-926X

<https://doi.org/10.1109/TAP.2004.838795>

---

**Reuse**

Unless indicated otherwise, fulltext items are protected by copyright with all rights reserved. The copyright exception in section 29 of the Copyright, Designs and Patents Act 1988 allows the making of a single copy solely for the purpose of non-commercial research or private study within the limits of fair dealing. The publisher or other rights-holder may allow further reproduction and re-use of this version - refer to the White Rose Research Online record for this item. Where records identify the publisher as the copyright holder, users can verify any specific terms of use on the publisher's website.

**Takedown**

If you consider content in White Rose Research Online to be in breach of UK law, please notify us by emailing [eprints@whiterose.ac.uk](mailto:eprints@whiterose.ac.uk) including the URL of the record and the reason for the withdrawal request.



[eprints@whiterose.ac.uk](mailto:eprints@whiterose.ac.uk)  
<https://eprints.whiterose.ac.uk/>

# A Smart Radar Absorber Based on the Phase-Switched Screen

Barry Chambers, *Senior Member, IEEE*, and Alan Tennant, *Member, IEEE*

**Abstract**—Although conventional (i.e., passive) radar absorbers are widely used for modifying the radar cross-section (RCS) of current military platforms, such absorbers may not have adequate performance to satisfy future requirements. Active absorbers, however, offer the potential to overcome the so-called Rozanov performance limit and to enable additional smart functionality such as monitoring damage, adaptive control of RCS or target appearance, identification-friend-or-foe, and absorb-while-scan. This paper outlines the concept and basic properties of a novel type of active radar absorber, the so-called phase-switched screen (PSS). The basic PSS topology is then modified so as to enable it to operate as a smart radar absorber when used together with an external sensor and feedback control loop. System implementation issues and the optimum choice of design parameters for a range of operational scenarios are discussed, and theoretical predictions are supported by measured performance data.

**Index Terms**—Electromagnetic scattering, modulation, radar absorbing material, radar cross-section.

## I. INTRODUCTION

ALTHOUGH conventional (i.e., passive) radar absorbers are widely used for modifying the radar cross-section (RCS) of current military platforms, such absorbers may not have adequate performance to satisfy some future requirements. For example, a passive radar absorber, once designed and manufactured, has fixed characteristics that are bounded by the electrical thickness at the lowest desired operating wavelength, following the so-called Rozanov limit [1]. Hence if the threat for which the absorber was designed changes, then either reduced performance against the new threat must be accepted or the material must be replaced by a better one. Active absorbers, however, offer the potential to overcome the Rozanov limit and to enable additional “smart” functionality such as monitoring damage, adaptive control of RCS or target appearance, identification-friend-or-foe, and absorb-while-scan [2].

Rozanov and earlier authors have shown that there are limitations to the performance of a particular absorber configuration and clearly these must apply to both passive and active absorbers since both obey the same laws of physics. However, although an active absorber, *in one particular electrical configuration*, is Rozanov-limited, it has the ability to change to a different configuration, which then has a different associated Rozanov limit. Hence an active absorber has the property that the sum of

its *instantaneous* bandwidths at a given reflectivity level is potentially larger than the Rozanov limit for the original passive absorber.

In general, passive and active absorbers rely on either destructive interference or the conversion of incident energy into heat; recently, however, a new type of active “absorber” has been proposed, the so-called phase-switched screen (PSS). Rather than absorbing the incident energy as heat, the PSS reflects it and spreads it over a very wide bandwidth using phase modulation. If this is done correctly, very little reflected energy will lie within the receiver bandwidth and thus the PSS exhibits the same behavior, *so far as the receiver is concerned*, as would an actual absorber. Although we have reported on a number of planar and conformal PSS configurations [3]–[12], in this paper we will consider only that based on a planar Salisbury screen in which the normal resistive sheet has been replaced by a layer whose conductance can be changed periodically with time in accordance with some externally applied electrical or optical stimulus. In the context of the discussion that follows, a smart absorber is defined as one that combines the attributes of incident field sensing, feedback, and electromagnetic reconfiguration. In the case of the active Salisbury screen configuration, the key to achieving smartness lies in replacing the perfectly conducting backplane by one that is “leaky.” In this paper, we consider how this concept may be used with a PSS rather than with the other types of active radar absorber discussed previously [2], [13]–[15].

Although several approaches may be used to explain the concept and basic properties of the PSS, here we will use that based on a transmission-line analog (TLA) of the absorber structure. This is valid for both continuous-wave and pulsed incident signals since in general the duration of an incident radar pulse is very long compared with the wave transit time through the absorber structure and the time for one-half cycle of the switching waveform used to control the active layer in the absorber. An analysis of the PSS based on the spectral approach is given in [9].

## II. BASIC THEORY OF THE SINGLE-LAYER PSS

The transmission-line analog of the single-layer PSS is shown in Fig. 1. It consists of a short-circuited length  $d$  of transmission line with characteristic admittance  $Y_c$  and propagation constant  $\beta$ , across whose input terminals is placed a conductance  $G(t)$ , defined as

$$\begin{aligned} G(t) &= G_1 & 0 < t < \tau \\ &= G_2 & \tau < t < T \end{aligned} \quad (1)$$

Manuscript received February 3, 2003; revised May 11, 2004.

The authors are with the Department of Electronic and Electrical Engineering, University of Sheffield, Sheffield S1 3JD, U.K. (e-mail: b.chambers@sheffield.ac.uk).

Digital Object Identifier 10.1109/TAP.2004.838795

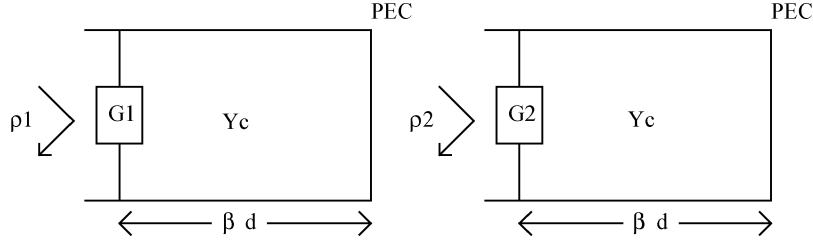


Fig. 1. Transmission-line analog of the PSS in its two states.

where  $\tau$  is the ON time and  $T$  is the time period for one cycle of the waveform used to control the state of  $G(t)$ . Depending on the incident polarization and angle of incidence  $\theta$ ,  $Y_c$  is given by either  $Y_0/\cos\theta$  for parallel polarization or  $Y_0\cos\theta$  for perpendicular polarization, where  $Y_0$  is the characteristic admittance of free-space. For either polarization,  $\beta$  is given by  $\beta = \beta_0\cos\theta$ . Thus, the input admittance of the PSS can assume one of two states—either  $Y_{in1}$  or  $Y_{in2}$ —given by

$$Y_{in1} = G_1 - jY_c \cot\beta d \quad \text{and} \quad Y_{in2} = G_2 - jY_c \cot\beta d. \quad (2)$$

These result in reflection coefficients  $\rho_1$  and  $\rho_2$ , which are related to  $Y_{in1}$  and  $Y_{in2}$  by

$$\rho_1 = \frac{Y - Y_{in1}}{Y + Y_{in1}} \quad \text{and} \quad \rho_2 = \frac{Y - Y_{in2}}{Y + Y_{in2}} \quad (3)$$

where  $Y = Y_0/\cos\theta$  or  $Y_0\cos\theta$  for parallel or perpendicular polarization, respectively. Since  $Y_{in1}$  and  $Y_{in2}$  are arbitrary, then  $\rho_1$  and  $\rho_2$  are generally complex.

For the PSS to behave like a perfect microwave absorber at a particular frequency, then the reflection coefficient  $\Gamma$ , when averaged over time  $T$ , must be equal to zero, i.e.,

$$\Gamma = \frac{1}{T} \int_0^T \rho(t) dt = 0. \quad (4)$$

For the case of ideal square-wave switching, this gives

$$\Gamma = \frac{1}{T} [\tau\rho_1 + (T - \tau)\rho_2] = 0 \quad (5)$$

which leads to the general admittance relation for the PSS. Thus, from (3) and (5) we have:

(a) parallel polarization

$$Y_{in1}Y_{in2} + \frac{Y_0}{\cos\theta} \left(1 - \frac{2\tau}{T}\right) (Y_{in2} - Y_{in1}) = \frac{Y_0^2}{\cos^2\theta} \quad (6)$$

(b) perpendicular polarization

$$Y_{in1}Y_{in2} + Y_0\cos\theta \left(1 - \frac{2\tau}{T}\right) (Y_{in2} - Y_{in1}) = Y_0^2\cos^2\theta. \quad (7)$$

In the simplest case when  $\tau = T/2$ , (6) and (7) become

$$Y_{in1}Y_{in2} = \frac{Y_0^2}{\cos^2\theta} \quad \text{and} \quad Y_{in1}Y_{in2} = Y_0^2\cos^2\theta \quad (8)$$

or, when written in terms of the switched conductances  $G_1$  and  $G_2$ :

(a) parallel polarization

$$\left[ G_1 - j\frac{Y_0}{\cos\theta} \cot(\beta_0 d \cos\theta) \right] \times \left[ G_2 - j\frac{Y_0}{\cos\theta} \cot(\beta_0 d \cos\theta) \right] = \frac{Y_0^2}{\cos^2\theta} \quad (9)$$

(b) perpendicular polarization

$$\left[ G_1 - jY_0\cos\theta \cot(\beta_0 d \cos\theta) \right] \times \left[ G_2 - jY_0\cos\theta \cot(\beta_0 d \cos\theta) \right] = Y_0^2\cos^2\theta. \quad (10)$$

If the incident frequency  $f_c$  is such that  $d\cos\theta = \lambda_c/4$ , then  $\beta_0 d \cos\theta = \pi/2$  and (9) and (10) simplify to

$$G_1G_2 = \frac{Y_0^2}{\cos^2\theta} \quad \text{and} \quad G_1G_2 = Y_0^2\cos^2\theta \quad (11)$$

respectively. Since the time-averaged reflection coefficient  $\Gamma$  is zero, the PSS behaves like a perfect absorber at  $f_c$ , as expected. When  $d\cos\theta \neq \lambda_c/4$ ,  $\Gamma$  will not in general be equal to zero but for the special case when  $\theta = 0^\circ$  and  $\tau = T/2$ , it is easy to show that  $\Gamma$  varies as  $\cos(\beta_0 d)$ . The more general case for oblique incidence is discussed elsewhere [8].

Hence, when  $\theta = 0^\circ$ , (11) gives the required relationship between the resistances of the PSS active layer in its two states, i.e.,

$$R_1R_2 = Z_0^2 \quad (12)$$

where  $R_1 = 1/G_1$ ,  $R_2 = 1/G_2$ , and  $Z_0 = 1/Y_0$ .

Equation (12) was derived independently for active radar absorbers in [4], but it has been reported previously in connection with diode-switched reflection phase shifters [16]. Although not mentioned in the literature, (12) also applies to the passive Salisbury screen, since it relates the two possible values of front sheet resistance which give a particular reflectivity null depth.

In principle there is an infinite number of pairs of resistance values that will satisfy (12), but in the experimental PSS described in [5], [6], and [11], the switched resistive layers took the form of a frequency selective surface (FSS) array consisting of dipole elements loaded by PIN diodes which were biased either fully on or fully off. Hence, to a good approximation over the bandwidth of the FSS,  $R_1 \approx 0\Omega$  and  $R_2 \approx \infty\Omega$ . Then

$\rho_1 \rightarrow -1$ ,  $\rho_2 \rightarrow +1$  and the time-averaged value of  $\Gamma \approx 0$  as expected, since the “on” time  $\tau$  was chosen to equal  $T/2$ .

As mentioned above, when  $d \neq \lambda_c/4$ , then  $\Gamma$  varies as  $\cos(\beta d)$ . Thus the bandwidth of the PSS is somewhat narrower than that of the Salisbury screen [9], and this behavior may be explained by considering the influence of multiple reflections inside the PSS structure. When  $R_1 = 0 \Omega$  and  $R_2 = \infty \Omega$ , the incident wave is only reflected from either the front or the back face of the PSS and no multiple reflections can occur. For other combinations of  $R_1$  and  $R_2$ , however, some of the wave incident on the front face of the PSS can always penetrate into its interior, thus giving rise to multiple reflections which will change the frequency characteristics. In the limiting case, when  $R_1 = R_2 = Z_0$ , then the frequency characteristics of the PSS become identical to those of the ideal Salisbury screen.

As we have seen, at resonance (i.e.,  $\beta_0 d = \pi/2$ ), the effect of switching  $R(t)$  between values  $R_1$  and  $R_2$ , as related by (11), mimics the reflectivity characteristics of a passive layer having a sheet resistance equal to  $Z_0$ . Hence it should be possible to adjust the effective sheet resistance  $R_{\text{eff}}$  by varying the “on” time  $\tau$  in each switching cycle. The relationship between  $R_{\text{eff}}$  and  $\tau$  is given by [4]

$$R_{\text{eff}} = Z_0 \frac{(T - \tau)}{\tau}. \quad (13)$$

Thus the PSS may be configured to act as a reflector or as a variable absorber simply by changing the duty cycle of the switching waveform applied to the active layer.

### III. EVOLUTION OF THE SMART PSS STRUCTURE

For the PSS to be made smart, it is necessary to modify its structure so as to facilitate two key requirements: incident field sensing and electromagnetic reconfiguration. Specifically, what we have in mind is a structure based on the PSS that has the ability to sense the frequency of an incident wave and to automatically place a reflectivity null of chosen depth onto that frequency so as to modify the target’s electromagnetic appearance to the incident wave. As mentioned before, the first requirement, that for incident field sensing, may be facilitated by making the PSS backplane “leaky” and by incorporating some form of frequency measuring element into the structure. The second requirement can be fulfilled by increasing the number of active layers in the PSS, thereby enabling simultaneous null depth and position control.

The first stage in the evolution of the smart PSS was the realization that the backplane could also be made active. The resulting bidirectional PSS (BPSS), shown in Fig. 2, is effective against illumination from either side of the structure and could thus be used in applications where the latter is electrically thin (e.g., a missile fin). In operation, the two active layers are switched in antiphase so that during a particular half-cycle of the switching waveform,  $R_{A1} \approx 0 \Omega$ ,  $R_{B1} \approx \infty \Omega$ , whereas during the next,  $R_{A2} \approx \infty \Omega$ ,  $R_{B2} \approx 0 \Omega$ , and so on. Then, irrespective of the value of  $\tau$ , the BPSS will have the same apparent reflectivity when viewed from either side (see [10, Fig. 4]).

In a previously reported implementation of a self-tuning radar absorber [2], [12], [13], sensing of the incident frequency was

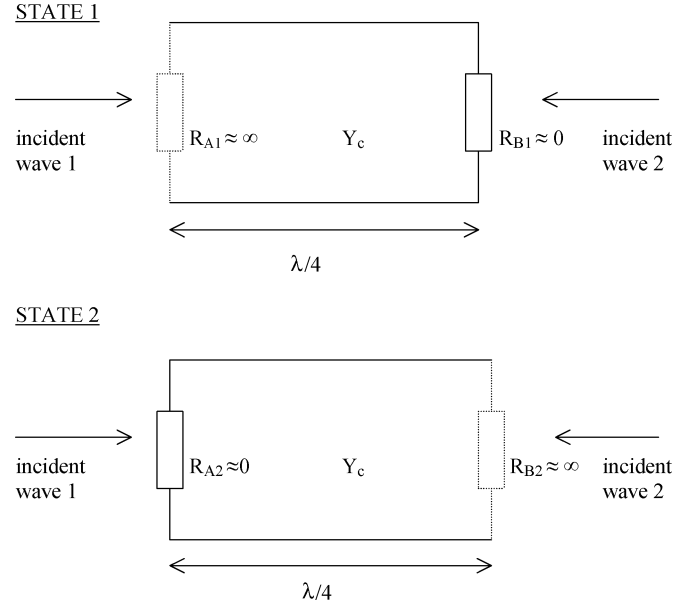


Fig. 2. Bidirectional phase-switched screen in its two operating states.

achieved by adding a tunable  $\lambda/2$  resonator section behind the absorber backplane (which was partially transparent). Although effective, this resulted in a structure that was  $3\lambda/4$  thick. When applying this technique to the PSS, however, it was realized that the  $\lambda/4$  thickness of the PSS is only used for half the time (i.e., when the active front layer resistance  $R_A = R_{A2} \rightarrow \infty \Omega$ . When  $R_{A1} \rightarrow 0 \Omega$ , the structure behind the active front layer can be used as one-half of the  $\lambda/2$  resonator section, as shown in Fig. 3(a). This results in a total structure thickness of only  $\lambda/2$  but does require  $R_{A1} > 0 \Omega$  so as to ensure that a small sample of the incident signal can pass through the  $\lambda/2$  resonator section and be detected. Since the general structure of the smart PSS, as shown in Fig. 3, is more complex than that of the single-layer PSS, shown in Fig. 1, (12) now relates the input resistances of the smart PSS in its two states, rather than the two values of the active layer resistance. Working in terms of  $G$  rather than  $R$ , for simplicity,  $G_{A1}$  and  $G_{A2}$  are now related by

$$G_{A2} = \frac{Y_0^2}{G_{A1} + \frac{Y_c^2}{G_{B1} + \frac{Y_c^2}{G_C + Y_L}}} - \frac{Y_c^2}{G_{B2} + \frac{Y_c^2}{G_C + Y_L}} \approx \frac{Y_0^2}{G_{A1} + G_C + Y_L} \quad (14)$$

where  $Y_L$  represents the loading of the PSS structure caused by the sensor at the output end of the  $\lambda/2$  resonator section. Since  $G_{A2}$  must be positive, this places restrictions on the values of the quantities appearing in (14), but in practice the latter will be satisfied if  $G_{B2} \rightarrow \infty$  (e.g.,  $R_{B2} \rightarrow 0 \Omega$ )

In summary, therefore, the final smart PSS structure is  $\lambda/2$  thick at the incident frequency and operates alternately in one of two states. In State 1, shown in Fig. 3(a), the resistance of the active front layer  $R_A$  is typically a few  $\Omega$  and the active layer defining the PSS backplane has a high resistance  $R_B$  (several tens of  $k\Omega$ ). For simplicity, the value of the back resistive layer  $R_C$  is set equal to  $R_A$ . The front and back resistive layers  $R_A$  and  $R_C$  thus define the boundaries of a  $\lambda/2$  resonator whose

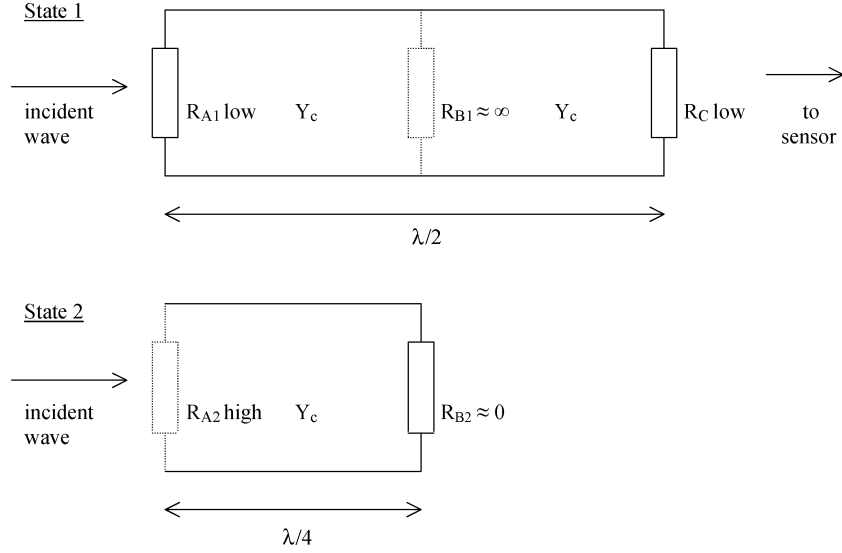


Fig. 3. Smart PSS in its two operating states.

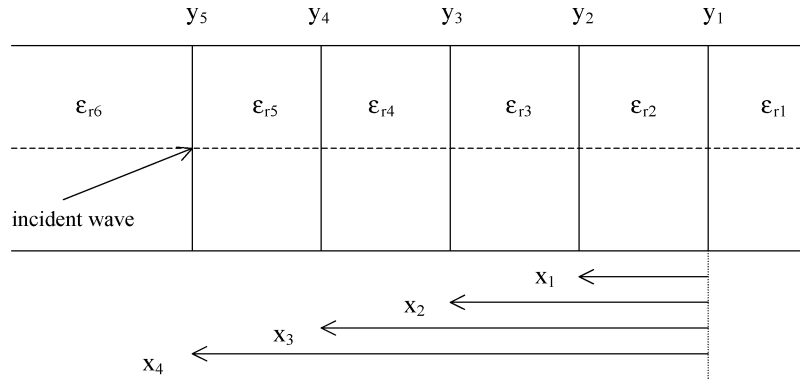


Fig. 4. Layer geometry of the smart PSS structure.

Q factor and insertion loss are determined by the value of  $R_A$ . In State 2, shown in Fig. 3(b),  $R_A$  is switched to a high value, determined from (14), and  $R_B$  is set low ( $\approx 0 \Omega$ ). In this state,  $R_C$  is left at its original value so as to ensure that transmission through the structure is low.

In the next section, we present a general analysis of the smart PSS structure and then use this to verify its reflection and transmission characteristics versus frequency.

#### IV. GENERAL THEORY OF THE SMART PSS

In this section, the smart PSS structure shown in Fig. 3 is generalized to include provision for reactive tuning elements. The resulting structure, shown in Fig. 4, is composed of five distributed sheet admittances  $y_1 - y_5$ , sandwiched between six dielectric layers, the first and last of which are assumed to be semi-infinite regions. The microwave reflection and transmission coefficients of this dielectric stack for arbitrary incidence angles and polarizations are readily obtained using multilayer stepping theory [17]. This involves the repeated use of the general transformer relationships between the incident, reflected, and transmitted wave amplitudes at the interface between the

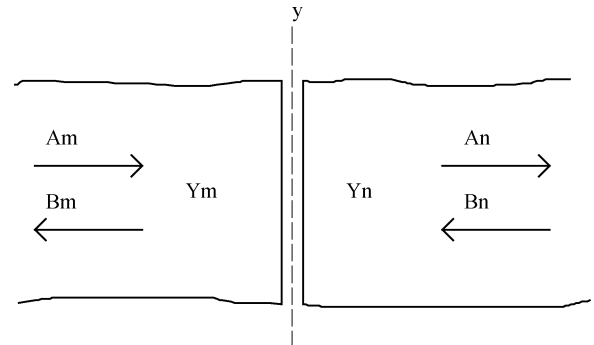


Fig. 5. Admittance sheet sandwiched between two dielectric layers.

$m$ th and  $n$ th layers, as shown in Fig. 5. The required equations for perpendicular incident polarization are

$$A_m = \frac{e^{jk_m x_n \cos \theta_m}}{2Y_m \cos \theta_m} \times [A_n(Y_m \cos \theta_m + Y_n \cos \theta_n + Y_n)e^{-jk_n x_n \cos \theta_n} + B_n(Y_m \cos \theta_m - Y_n \cos \theta_n + Y_n)e^{jk_n x_n \cos \theta_n}] \quad (15)$$

and

$$B_m = \frac{e^{-jk_m x_n \cos \theta_m}}{2Y_m \cos \theta_m} \times [A_n(Y_m \cos \theta_m - Y_n \cos \theta_n - Y_n)e^{-jk_n x_n \cos \theta_n} + B_n(Y_m \cos \theta_m + Y_n \cos \theta_n - Y_n)e^{jk_n x_n \cos \theta_n}] \quad (16)$$

and those for parallel incident polarization are

$$A_m = \frac{e^{jk_m x_n \cos \theta_m}}{2Y_m \cos \theta_m} \times [A_n(Y_m \cos \theta_n + Y_n \cos \theta_m + Y_n \cos \theta_m \cos \theta_n)e^{-jk_n x_n \cos \theta_n} + B_n(Y_m \cos \theta_n - Y_n \cos \theta_m + Y_n \cos \theta_m \cos \theta_n)e^{jk_n x_n \cos \theta_n}] \quad (17)$$

and

$$B_m = \frac{e^{-jk_m x_n \cos \theta_m}}{2Y_m \cos \theta_m} \times [A_n(Y_m \cos \theta_n - Y_n \cos \theta_m - Y_n \cos \theta_m \cos \theta_n)e^{-jk_n x_n \cos \theta_n} + B_n(Y_m \cos \theta_n + Y_n \cos \theta_m - Y_n \cos \theta_m \cos \theta_n)e^{jk_n x_n \cos \theta_n}] \quad (18)$$

where  $y_n$  is the admittance of an impedance ( $R$  or  $C$ ) sheet placed between the  $m$ th and  $n$ th layers in the stack  $x_n$  is the location of the  $n$ th interface, and  $\theta_m$  and  $\theta_n$  are the angles of incidence and refraction at the  $n$ th interface. The characteristic admittances of the  $m$ th and  $n$ th layers in the stack  $Y_m$  and  $Y_n$  will be determined by the layer parameters  $\varepsilon$  and  $\mu$  together with the values of  $\theta_m$  and  $\theta_n$ . Equations (15) and (16) or (17) and (18) are used iteratively to find  $A_6$  and  $B_6$  at the front of the stack (i.e., the PSS front face) from arbitrarily chosen starting conditions at the back of the stack, namely,  $A_1 = 1$ ,  $B_1 = 0$  (i.e., the sensor is matched).

The structure reflection coefficient is then defined in terms of  $A_6$  and  $B_6$  as

$$\rho = \frac{B_6}{A_6} \quad (19)$$

and the transmission coefficient through the structure is given by

$$\Lambda = \frac{A_1}{A_6} = \frac{1}{A_6}. \quad (20)$$

To determine the time-averaged reflectivity of the PSS, (19) is used to determine  $\rho$  for the structure in its two states. These are then combined using (5), i.e.,

$$\text{Reflectivity (dB)} = 20 \log_{10} (|\tau' \rho_1 + (1 - \tau') \rho_2|) \quad (21)$$

where

$$\tau' = \frac{\tau}{T}. \quad (22)$$

Similarly, the time-averaged insertion loss of the  $\lambda/2$  resonator is given by

$$\text{Insertion Loss (dB)} = -20 \log_{10} (|\tau' \Lambda_1 + (1 - \tau') \Lambda_2|). \quad (23)$$

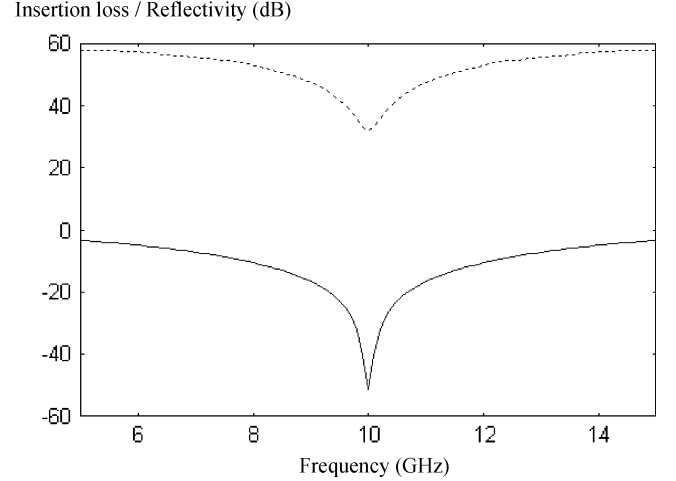


Fig. 6. Reflectivity and insertion loss characteristics of fixed-tuned smart PSS  $R_{A1} = R_C = 10 \Omega$ ,  $R_{B1} = 1 M\Omega$ ,  $R_{A2} = 28380 \Omega$ ,  $R_{B2} = 1 \Omega$ ,  $d = 7.5$  mm --- insertion loss, — reflectivity.

As a check on the validity of the above theory, (21)–(23) were used to calculate the frequency characteristics of an ideal fixed-tuned smart PSS structure in free-space which was 15 mm thick (i.e.  $\lambda/2$  at 10 GHz with spacer  $\varepsilon_r = 1$ ) and with  $R_{A1} = R_C = 10 \Omega$ ,  $R_{A2} = 28380 \Omega$ ,  $R_{B1} = 1 M\Omega$ ,  $R_{B2} = 1 \Omega$ , and  $Z_L = 376.7 \Omega$ . As can be seen from Fig. 6, the curves of reflectivity and insertion loss have the desired characteristics, with a deep reflectivity null and minimum insertion loss both occurring at the desired frequency. In the next section, we consider how best to tune the smart PSS and the optimum choice of  $R_{A1}$  (and hence  $R_C$ ).

## V. SYSTEM ASPECTS

### A. Smart PSS Tuning

In a normal  $\lambda/2$  transmission line resonator, the optimum position for a tuning capacitor would be at the high impedance point, i.e., in the middle of the resonator. In the smart PSS structure, however, tuning must be achievable for both the  $\lambda/2$  resonator (when in State 1) and the PSS (when in State 2). Furthermore, the apparent capacitance in each state must be such that the reflectivity null frequency and the minimum insertion loss frequency “track” together. This can only be achieved if the PSS is tuned by a capacitor placed at its midpoint position, i.e.,  $\lambda/8$  from the active front face, and the resonator is tuned by this same capacitor and its twin which is placed  $\lambda/8$  from the structure back face. Only then will these capacitors experience the same local line impedance in both states of the structure. Obviously, two capacitors are needed to tune the resonator section correctly since it has twice the electromagnetic “volume” of the PSS. The resulting structure of the tunable smart PSS is shown in Fig. 7. Fig. 8 shows the reflectivity and insertion loss characteristics of the structure, with the same resistance values as used for Fig. 6, but when the ideal tuning capacitors  $C_A$  and  $C_B$  each have values of 0, 50, 100, and 200 fF, respectively. The curves for  $C_A = C_B = 0$  fF are identical in shape to those shown in Fig. 6, but the additional null in the insertion loss curve at 20 GHz should be noted. This is merely due to the

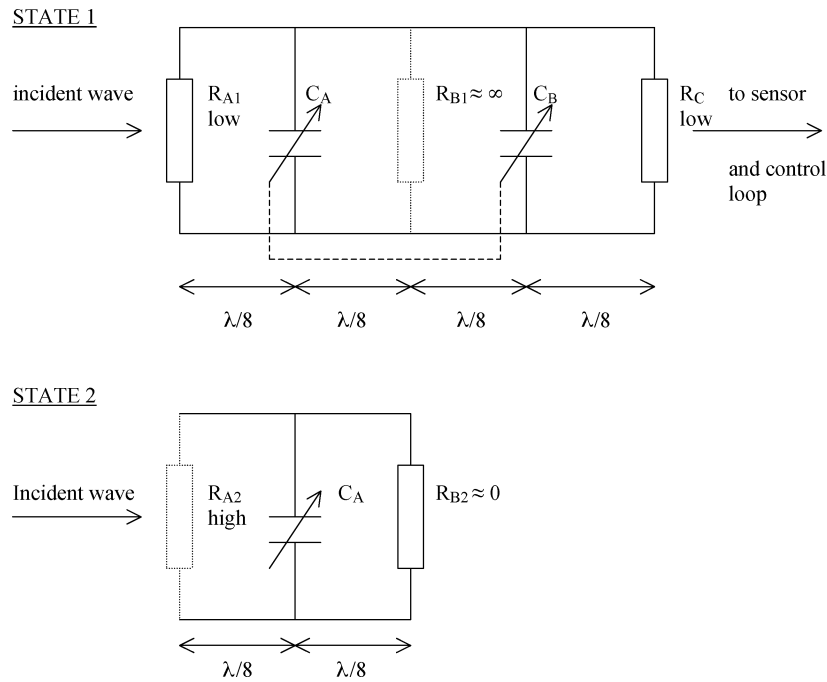
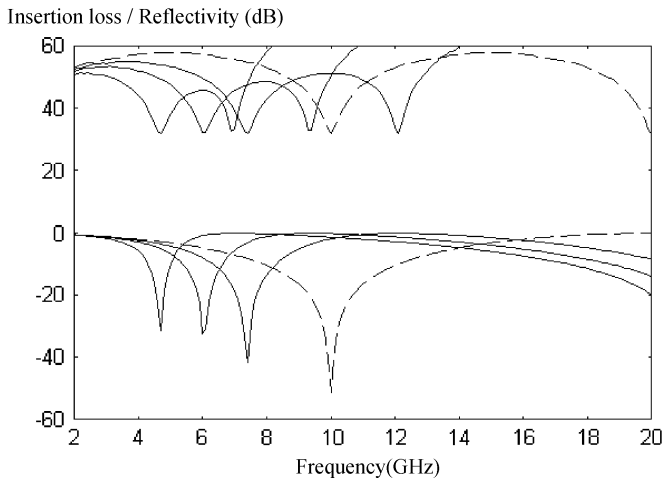
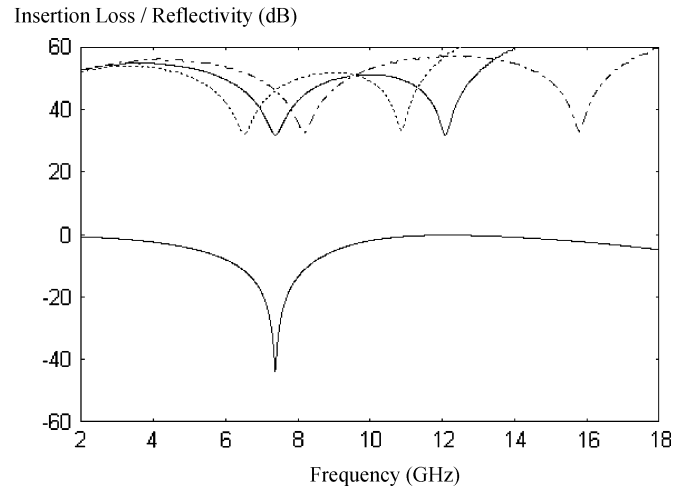


Fig. 7. Tunable smart PSS structure in its two operating states.


 Fig. 8. Tuning and tracking characteristics of smart PSS —  $C_A = C_B = 0$  fF, solid lines are for  $C_A = C_B = 50, 100,$  and  $200$  fF, respectively.

 Fig. 9. Behavior of smart PSS in absorb-while-scan mode solid lines are for  $C_A = C_B = 50$  fF, —  $C_B = 0$  fF, - - -  $C_B = 100$  fF.

resonator now being  $\lambda$  in length. When  $C_A = C_B > 0$ , two features in the curves are apparent. First, the reflectivity null and minimum insertion loss frequencies do indeed track correctly, but the second resonance point in the insertion loss curve has moved much closer to the fundamental resonance point. This has occurred since the tuning capacitors are at the ideal positions for tuning the resonator at its second harmonic, rather than at the desired fundamental frequency. This should not cause any problems, however, since the two resonances are still well separated for any values of capacitance that are likely to be used in practice.

The above discussion has assumed that the incident wave is normal to the PSS front face. For the case of oblique incidence, however, correct frequency tracking between the PSS and the resonator will still occur since the electrical length of both structures is defined similarly in terms of  $\theta$ . A discussion of how the

PSS should be switched so as to be effective against both incident polarizations simultaneously is given in [8].

### B. Absorb-While-Scan Mode of Operation

In Section V-A, we considered the behavior of the smart PSS when the two tuning capacitors  $C_A$  and  $C_B$  had the same value. In a given situation, once the PSS reflectivity null has been tuned onto a threat frequency  $f_1$ , it is possible to keep  $C_A$  fixed (so as to keep the reflectivity null at  $f_1$ ) and to tune the resonator *independently* by changing the value of  $C_B$ , as shown in Fig. 9. By this means, the smart PSS structure may be used to search for a second threat frequency  $f_2$  while simultaneously dealing with the first; this mode of operation is termed *absorb-while-scan*. If a second threat frequency of higher priority is found when  $C_B = C$ , the PSS reflectivity null may be retuned to this by setting  $C_A = C_B = F(C_A, C)$ , where the function  $F$  may

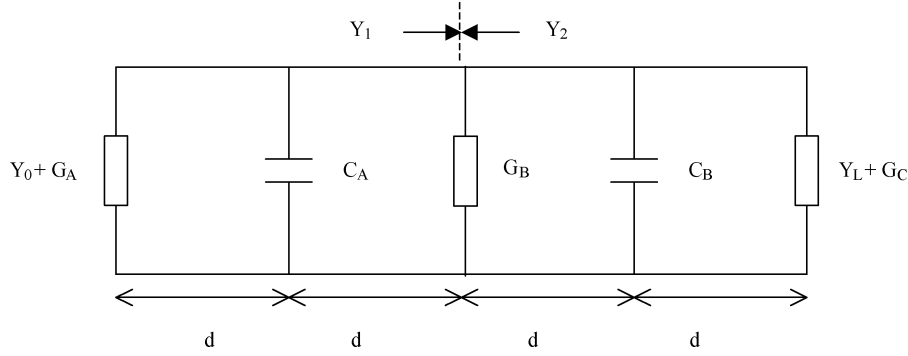


Fig. 10. Calculation of resonance conditions for absorber and resonator sections of the smart PSS structure.

be determined using the transverse-resonance technique [18]. Starting with the equivalent circuit of the smart PSS in State 1, as shown in Fig. 7, the resonator is assumed to be terminated at its input by a parallel combination of  $Y_0$  and  $G_A$  and at its output by a parallel combination of  $Y_L$  and  $G_C$ , as shown in Fig. 10. Then we may equate the local admittances  $Y_1$  and  $Y_2$  seen on either side of some arbitrary reference plane within the resonator. This leads to a general equation that gives the resonant frequency  $f_{\text{res}}$ , for known values of  $C_A$  and  $C_B$  (since in general  $C_A \neq C_B$ ). When the reference plane is positioned at the center of the resonator, we obtain

$$G_B + Y_C \frac{(Y_1' + jY_c \tan \beta d)}{(Y_c + jY_1' \tan \beta d)} + Y_c \frac{(Y_2' + jY_c \tan \beta d)}{(Y_c + jY_2' \tan \beta d)} = 0 \quad (24)$$

where

$$Y_1' = j\omega C_B + \frac{Y_c(G_C + Y_L + jY_c \tan \beta d)}{Y_c + j(G_C + Y_L) \tan \beta d} \quad (25)$$

$$Y_2' = j\omega C_A + \frac{Y_c(G_A + Y_0 + jY_c \tan \beta d)}{Y_c + j(G_A + Y_0) \tan \beta d} \quad (26)$$

and  $\omega = 2\pi f_{\text{res}}$ .

$f_{\text{res}}$  may then be substituted back into (24) to find the value of two new identical capacitors  $C'_A$  and  $C'_B$ , which will again tune the resonator to  $f_{\text{res}}$ . It is the new capacitor  $C'_A$  that is then used to position the PSS reflectivity null at the new threat frequency  $f_2 = f_{\text{res}}$ .

As an example, if  $R_{A1} = R_C = 10 \Omega$ ,  $R_{B1} = 30 \text{ K}\Omega$ ,  $R_L = 376.7 \Omega$ ,  $R_{1B} = 2 \Omega$ , and  $d = 3.5 \text{ mm}$ , then from (14),  $R_{A2} = 36256 \Omega$ . Let the initial threat frequency  $f_1 = 9.917 \text{ GHz}$ ; then from (24), the PSS absorber and resonator sections can be tuned to this by setting  $C_A = C_B = 10 \text{ fF}$ . If a new threat now occurs at frequency  $f_2 = 8.49 \text{ GHz}$ , the resonator will sense this when  $C_A$  is still set to  $10 \text{ fF}$  (so that the PSS null is still at  $f_1$ ) and  $C_B$  is then set to  $50 \text{ fF}$ . Subsequently, the PSS absorber null can then be reset to deal with  $f_2$  by setting  $C_A$  and  $C_B$  to  $33.65 \text{ fF}$ . This process can be repeated as often as desired, but is only effective against a relatively slowly changing threat scenario. The technique cannot be used to synthesise a broadband absorber characteristic, e.g., giving a  $-20 \text{ dB}$  reflectivity performance at say 100 spot frequencies “simultaneously” because each frequency can only be visited for  $1/100$  of the available time and hence the time-averaged performance over the total bandwidth is degraded by a factor of 100.

Insertion loss (dB)

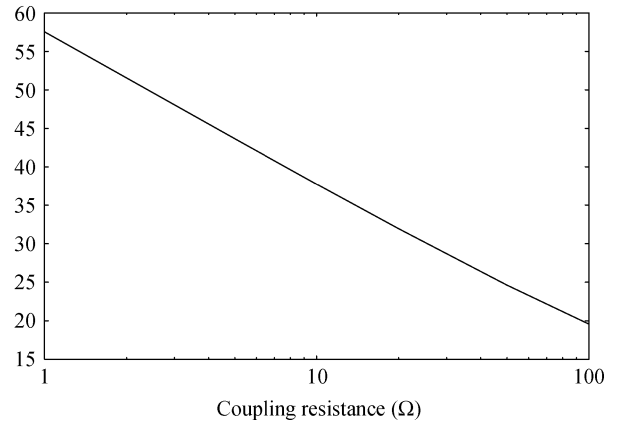


Fig. 11. Dependence of smart PSS resonator insertion loss on coupling resistance  $d = 15 \text{ mm}$ ,  $f = 10 \text{ GHz}$ ,  $Z_0 = 376.7 \Omega$ .

### C. Choice of $\lambda/2$ Resonator Coupling Resistances

It is necessary to consider the optimum value for the  $\lambda/2$  resonator coupling resistances for several reasons. First, this will have an effect on the resonator Q factor and insertion loss, but secondly, it will also have important implications for system implementation, when the smart PSS is used in conjunction with a detector and feedback control loop.

Fig. 11 shows the variation of minimum resonator insertion loss with coupling resistance  $R$  as calculated using (23). The corresponding unloaded Q-factor may be calculated from [18]

$$Q \approx \frac{\pi Z_0}{4R}. \quad (27)$$

A further consideration is that of the relative signal magnitudes received by a radar, via backscatter from a PSS-covered target, and by the PSS sensor, via transmission through the structure. The signal received at a monostatic radar via backscatter from a PSS-covered target having a radar cross-section  $\sigma$  is given approximately by

$$S_1 = \frac{P_T G_T G_R \sigma \lambda^2}{64\pi^3 D^4} \quad (28)$$

where  $P_T$  is the radar transmitter output power,  $G_T = G_R$  is the gain of the radar antenna,  $D$  is the range from the radar to the target, and  $\lambda$  is the operating wavelength. For simplicity, assume that the radar and smart PSS receivers have the same sensitivity;

TABLE I  
(a)  $\sigma = 0$  dBsm,  $G_R/G_S = 100$  (b)  $\sigma = -20$  dBsm,  $G_R/G_S = 100$

D (km)	Maximum value of $T_L$ (dB)	D (km)	Maximum value of $T_L$ (dB)
1	51	1	71
10	71	10	91
50	85	50	105
100	91	100	111
200	97	200	117
300	103	300	123

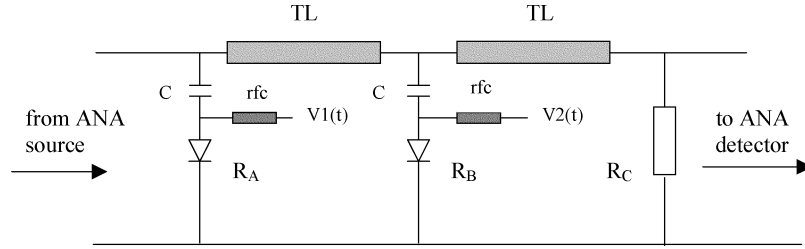


Fig. 12. Experimental lumped circuit analog of fixed-tuned smart PSS structure  $C =$  dc blocking capacitor,  $TL = 80$  mm length of RG402 coaxial cable ( $Z_0 = 50 \Omega$ ), rfc = radio frequency choke,  $R_A = R_B =$  BAP64 PIN diode,  $R_C = 1.2 \Omega$  (nominal).

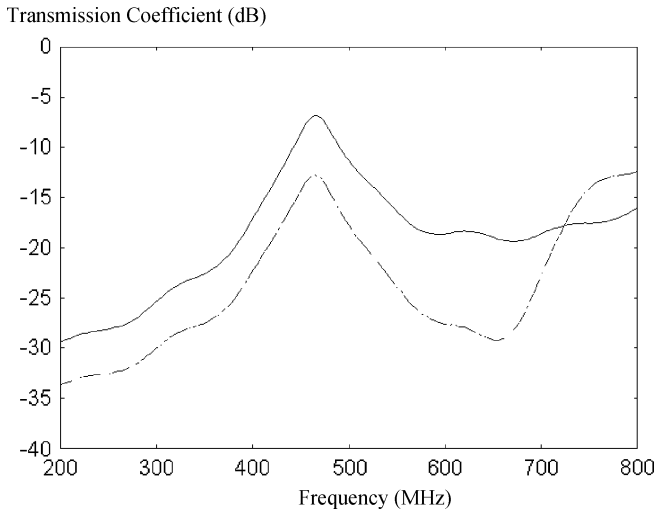


Fig. 13. Measured transmission characteristics of PSS resonator in switched and unswitched states,  $R_A$  represented by PIN diode with  $I_F = 5$  mA,  $R_C = 1.2 \Omega$  (nominal) —  $R_B$  diode off, - - -  $R_B$  diode switched with 50% duty cycle square wave.

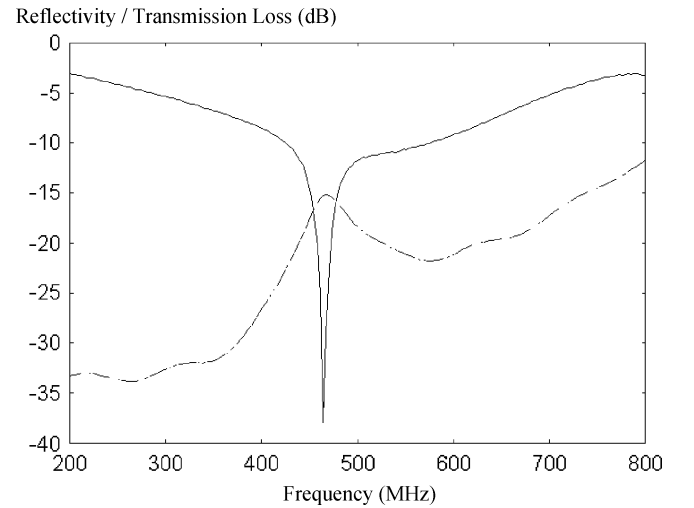


Fig. 14. Synthesized reflectivity (—) and transmission loss (- - -) characteristics of transmission-line analog of fixed-tuned smart PSS structure,  $\tau = 0.5 T$ . State 1: front diode  $I_F = 5$  mA, back diode  $I_F = 0$ . State 2: front diode  $I_F = 50 \mu$ A, back diode  $I_F = 5$  mA.

then the signal received by the PSS sensor from the radar is given by

$$S_2 = \frac{P_T G_T G_S \lambda^2}{16\pi^2 d^2 \Lambda} \quad (29)$$

where  $G_S$  is the gain of the PSS sensor antenna and  $\Lambda$  is the transmission loss through the PSS, as given by (20).

In practice, it is required that  $S_1 \ll S_2$ . Hence from (28) and (29)

$$\Lambda \ll \frac{4\pi d^2 G_S}{\sigma G_R}. \quad (30)$$

The upper limit on the transmission loss through the smart PSS structure  $T_L$ (dB) may now be established from (30) and some results are shown in Table I.

From Table I, it can be seen that a reasonable choice for  $T_L$  might be 40 dB and hence from Fig. 11, our previous choice of  $R_{A1} = 10 \Omega$  is appropriate. From (27), this implies an unloaded resonator Q of about 30, which should be adequate in practice. A higher value of Q could of course be obtained by decreasing the value of  $R_{A1}$ , but this would not only increase the resonator insertion loss and hence require careful reconsideration of the results predicted from (30) but might also lead to a more stringent design of the feedback control loop, which might have implications for the system response time. This is an area for future consideration.

## VI. EXPERIMENTAL APPARATUS AND MEASURED RESULTS

In our previous work on the PSS, theoretical predictions have been confirmed by measurements made on structures based on both transmission-line analogs and large area diode-loaded FSS

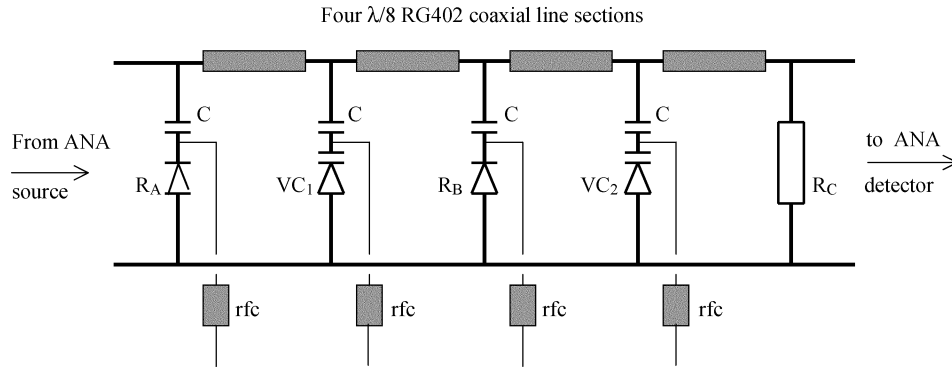


Fig. 15. Experimental lumped circuit analog of smart PSS structure  $C =$  dc blocking capacitor,  $VC =$  BB833 varactor diode,  $rfc =$  radio frequency choke,  $R_B = R_B =$  BAP64 PIN diode,  $R_C = 1.2 \Omega$  (nominal).

operating in free-space. In the case of the smart PSS, the structure requires a total of four active layers, and so before committing ourselves to the large expenditure required for building such a complex large-area structure for free-space operation, it was decided to try and confirm some of the theoretical predictions discussed above using lumped-circuit analogues of the smart PSS structure operating at ultrahigh frequency. The switched resistive layers were each represented by a Philips BAP64 silicon PIN diode and the  $\lambda/4$  spacers were constructed from 80 mm lengths of RG402 semirigid coaxial cable ( $Z_0 = 50 \Omega$ ). An Agilent 8714B vector network analyzer was used to simulate an incident plane wave and the smart PSS detector.

Before carrying out reflection and transmission measurements on the fixed-tuned PSS structure shown in Fig. 12, a test was made to confirm the behavior of the resonator section as predicted by (23). With  $R_C$  fixed at  $1.2 \Omega$  and the PIN diode representing  $R_B$  unbiased, the forward current  $I_F$  through the PIN diode representing  $R_A$  was increased until a clearly defined resonance curve was obtained. This occurred for values of  $I_F$  greater than about 2.5 mA but, as expected, larger values of  $I_F$  produced higher resonator Q factors and insertion losses. In a practical large-area PSS panel, there would need to be a tradeoff between these resonator properties and power consumption, as represented by diode  $I_F$ ; accordingly,  $I_F$  was fixed at 5 mA and the PIN diode representing  $R_B$  was driven by a square-wave voltage waveform having a 50% duty cycle (i.e.,  $\tau/T = 0.5$ ). From Fig. 13, it can be seen that as predicted, the measured resonator insertion loss increases by approximately 6 dB when the state of  $R_B$  changes from being permanently high (i.e., diode off) to being switched alternately high and low by the square-wave bias.

Correct switching of the smart PSS structure between States 1 and 2 requires a dual output pulse generator whose outputs are complementary but of unequal magnitude and dc shift; because such a generator was not available to us, the transmission and reflection characteristics of the smart PSS structure were synthesized in a computer using (21) and (23) and measured complex transmission and reflection data for the two states of the structure when appropriate dc currents flowed through the two diodes. This approach is valid since in practice the diode response time is very much shorter than the switching period  $T$ . For consistency, the forward current for each diode in its low resistance state was set at  $I_{F(\text{low})} = 5$  mA and a series of reflection and transmission measurements were taken for various values of  $I_F$  for the

Reflectivity/Transmission loss (dB)

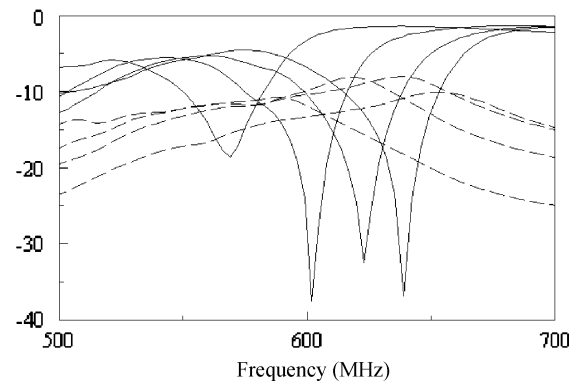


Fig. 16. Synthesized reflectivity (—) and transmission loss (---) characteristics of tunable smart PSS structure Varactor diode bias varied in 1 V steps from 5 to 8 V, other conditions as for Fig. 15.

diode representing  $R_A$  in its high resistance state. On processing this data, it was found that optimum smart PSS performance was obtained for  $I_{F(\text{high})} = 50 \mu\text{A}$  and the resulting PSS characteristics are shown in Fig. 14. These confirm the basic behavior of the smart PSS structure since the reflectivity null frequency is almost exactly coincident with the bandpass filter center frequency. Although not shown here, other data were taken with  $I_{F(\text{low})} = 10$  mA and these gave very similar results.

A tunable transmission-line analog of the smart PSS structure was next constructed as shown in Fig. 15. The  $\lambda/8$  spacers were represented by 40 mm lengths of RG 402 coaxial cable and Infineon BB833 varactor diodes were used as the tunable capacitive elements. Using the same PIN diode biasing conditions as before, a series of measurements was taken with both variable capacitance diodes biased identically in 1 V steps from 5 to 8 V. Using these data, typical synthesized reflection and transmission characteristics of the tunable smart PSS structure are shown in Fig. 16. As expected, increasing the value of the tuning capacitances reduced the reflectivity null and minimum transmission loss frequencies, but close examination of the data plotted in Fig. 16 shows that there is an almost constant tracking error between corresponding reflection and transmission curves. Further experimental work and computer modeling suggests that this tracking error is due to slight differences in the C–V characteristics of individual varactor diodes; in practice this could be compensated for by calibration and the use of a lookup table in the smart PSS control software [15].

## VII. CONCLUSION

In this paper, we have introduced the concept of the phase-switched screen and examined how this may be reconfigured to act as a smart radar absorber. Theoretical predictions have been supported using transmission-line analogs of the smart structure operating under open-loop conditions. It is now intended to investigate operation of a large-area smart PSS structure operating in free-space under both open- and closed-loop conditions [15] and this work will be reported elsewhere.

## REFERENCES

- [1] K. N. Rozanov, "Ultimate thickness to bandwidth ratio of radar absorbers," *IEEE Trans. Antennas Propag.*, vol. 48, pp. 1230–1234, 2000.
- [2] B. Chambers, "A smart radar absorber," *Smart Mater. Struct.*, vol. 8, pp. 64–72, 1999.
- [3] A. Tennant, "Reflection properties of a phase modulating planar screen," *Electron. Lett.*, vol. 33, pp. 1768–1769, 1997.
- [4] B. Chambers, "Characteristics of modulated planar radar absorbers," *Electron. Lett.*, vol. 33, pp. 2073–2074, 1997.
- [5] A. Tennant and B. Chambers, "Experimental phase modulating planar screen," *Electron. Lett.*, vol. 34, pp. 1143–1144, 1998.
- [6] —, "Experimental two-layer adaptive phase-switched screen," *Electron. Lett.*, vol. 37, pp. 1379–1380, 2001.
- [7] —, "Bistatic scattering from cylindrical phase switched screens," *Electron. Lett.*, vol. 37, pp. 1507–1509, 2001.
- [8] P. N. Kaleeba, A. Tennant, and J. P. Ide, "Characteristics of phase-switched screens at oblique incidence," in *Proc. AMTA 2001*, Boulder, CO, pp. 177–182.
- [9] B. Chambers and A. Tennant, "Influence of switching waveform characteristics on the performance of a single layer phase-switched screen," *IEEE Trans. Electromagn. Compat.*, vol. 44, pp. 434–441, Aug. 2002.
- [10] —, "General analysis of the phase-switched screen, part 1: the single layer case," *Proc Inst. Elect. Eng. F—Radar Sonar Nav.*, vol. 149, pp. 243–247, 2002.
- [11] A. Tennant and B. Chambers, "An experimental dual-polarized phase switched screen," *Electron. Lett.*, vol. 39, pp. 119–121, 2003.
- [12] —, "Experimental broadband single layer PSS using reactive impedance switching," *Electron. Lett.*, vol. 39, pp. 121–122, 2003.
- [13] B. Chambers, "Internal monitoring of the frequency response of a dynamically-adaptive radar absorbing material," *Electron. Lett.*, vol. 32, pp. 1711–1712, 1996.
- [14] —, "Dynamically-adaptive radar absorbing material with improved self-monitoring characteristics," *Electron. Lett.*, vol. 33, pp. 529–530, 1997.

- [15] K. L. Ford and B. Chambers, "Smart microwave absorber," *Electron. Lett.*, vol. 36, pp. 50–52, 2000.
- [16] H. V. Shurmer, *Microwave Semiconductor Devices*. New York: Pitman, 1971.
- [17] E. F. Knott, J. F. Schaeffer, and M. T. Tuley, *Radar Cross Section*, 2nd ed. Boston, MA: Artech House, 1993.
- [18] R. E. Collin, *Foundations for Microwave Engineering*. New York: McGraw-Hill, 1966.

**Barry Chambers** (SM'99) received the B.Eng. degree in electrical engineering and the Ph.D. and D.Eng. degrees from the University of Sheffield, U.K., in 1964, 1968, and 2002, respectively.

In 1968, he joined the Department of Electrical Engineering, University of British Columbia, Vancouver, ON, Canada, as a postdoctoral Teaching Fellow and was appointed Assistant Professor there in 1969. In 1971, he returned to the University of Sheffield, where he is now Professor of communication engineering and Head of the Communications and Radar Group. His current research interests include evolutionary optimization techniques, synthesis and applications of nanocomposite polymer materials with novel electromagnetic properties, electromagnetic wave scattering, low observable techniques and technology, smart electromagnetic structures, and automated microwave metrology. He has published more than 170 scientific journal and conference papers and has contributed to three books.

Dr Chambers is a Fellow of the Institution of Electrical Engineers, where he has served on the Professional Group Committees for Antennas and Propagation and for Radar, Sonar and Navigation. He is currently a member of the Institution of Electrical Engineers' Professional Network Technical Panel for Antennas and Propagation.

**Alan Tennant** (M'03) received the B.Eng. degree in electronic engineering and the Ph.D. degree in medical physics from the University of Sheffield, U.K., in 1985 and 1992, respectively.

Between 1985 and 1986, he was with BAe Systems, Stevenage, U.K. In 1992, he joined the Defence and Evaluation Research Agency (DERA), Malvern, U.K., where he worked on phased array antenna systems, before taking up an academic post at the University of Hull, U.K. In 2001, he returned to the University of Sheffield as a Senior Lecturer in the Communications and Radar Group. His research interests include adaptive materials for radar signature management, novel 3-D phased array antenna topologies, and acoustic array systems.